BNL-226018-2024-JAAM

Mechanocatalytic Hydrogenolysis of the Lignin Model Dimer Benzyl Phenyl Ether over Supported Palladium Catalysts

E. Phillips, E. Stavitski

To be published in "ACS Sustainable Chemistry & Engineering"

August 2024

Photon Sciences

Brookhaven National Laboratory

U.S. Department of Energy

USDOE Office of Science (SC), Basic Energy Sciences (BES)

DISCLAIMER

ACS Sustainable Chemistry & Engineering

pubs.acs.org/journal/ascecg

Letter

Mechanocatalytic Hydrogenolysis of the Lignin Model Dimer Benzyl Phenyl Ether over Supported Palladium Catalysts

Erin V. Phillips, Andrew W. Tricker, Eli Stavitski, Marta Hatzell, and Carsten Sievers*

Cite This: *ACS Sustainable Chem. Eng.* 2024, 12, 12306−12312

Read Online

ACCESS | Metrics & More | Article Recommendations | Supporting Information

ABSTRACT: This work demonstrates the mechanocatalytic hydrogenolysis of the ether bond in the lignin model compound benzyl phenyl ether (BPE) and hardwood lignin isolated by hydrolysis with supercritical water. Pd catalysts with 4 wt % loading on Al_2O_3 and SiO_2 supports achieve 100% conversion of BPE with a toluene production rate of (2.6−2.9) × 10^{-5} mol·min^{-1}. The formation of palladium hydrides under H_2 gas flow contributes to an increase in the turnover frequency by a factor of up to 300 compared to Ni on silica−alumina. While a near-quantitative toluene yield is obtained, some of the phenolic products remain adsorbed on the catalyst.

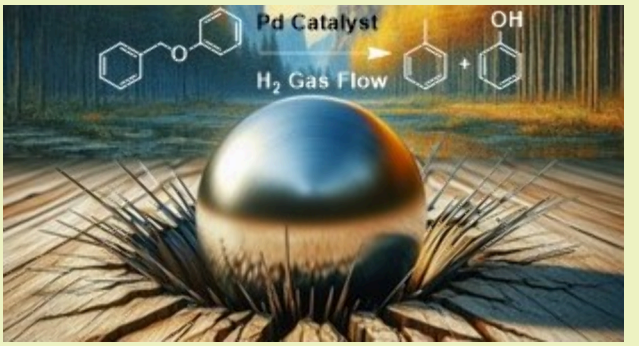

KEYWORDS: *ball mill, biomass conversion, depolymerization, heterogeneous catalysis, lignin model compounds, mechanochemistry*

Lignin, a major component of lignocellulosic biomass, is the most abundant source of aromatics in nature but remains significantly underutilized due to lignin's complex and amorphous structure.[1−5] The three-dimensional polymer is composed of substituted phenolic monomers, called monolignols, that contain a variable number of hydroxy and methoxy groups and a propyl side chain. A variety of ether, alkyl, or aryl bonds connect the monomers. These bonds are difficult to selectively cleave, resulting in the recalcitrant and chemically diverse structure of lignin. Various approaches, such as pyrolysis and reductive catalytic fractionation (RCF), have been used to depolymerize lignin to its aromatic components, but each method presents a unique set of complications. Pyrolysis is energy-intensive due to the high temperatures required, while RCF can only be applied to unfractionated lignocellulosic biomass and is often associated with coking issues and the repolymerization of intermediates to unreactive polyaromatics.[6−11] Due to incomplete bond cleavage and repolymerization, monomer yields resulting from RCF typically do not exceed ∼55% even under optimized conditions.[12] Hydrogenolysis specifically targets the cleavage of carbon−carbon or carbon−heteroatom bonds, followed by stabilization via the addition of an H atom.[6−8] Homogenous catalysts can effectively cleave ether bonds in lignin, but difficult separations and low product purity are common disadvantages.[8] Alternatively, solid catalysts, such as supported Ni, Pd, or Pt, allow for easier separation under reasonably mild conditions, but contacting them with a solid feedstock like lignin that is insoluble in most common solvents is a significant challenge.[7,8,12−14] Pd was specifically chosen as the primary active metal for this study due to its ability to form interstitial hydrides as a hydrogen storage reservoir, which is advantageous in facilitating hydrogenolysis reactions.[15−17]

Mechanocatalysis is an emerging approach that utilizes either the vibrational or rotational forces in a ball mill or similar device to drive reactions in a solvent-free environment.[18−23] Compared to other traditional methods for lignin conversion, such as pyrolysis, mechanocatalysis is an attractive alternative because no additional heating or pressurization is required to complete many reactions.[19,20,24,25] A variety of phenomena have been considered as potential drivers for mechanochemical reactions including the formation of thermal hot spots upon impact between the balls and vessel walls, highly active transient sites on a mechanically excited catalyst surface, and increased solid−solid contact between the solid feedstock and catalyst particles as a result of consistent mixing and shearing.[19,26,27]

Several studies of mechanocatalysis as an approach to depolymerizing lignocellulosic biomass and lignin model compounds have been conducted.[5,14,28−43] Rinaldi et al. demonstrated the depolymerization of both cellulose and biomass to water-soluble sugars and furfurals with complete conversion and yields of water-soluble oligosaccharides and lignin oligomers exceeding 90%.[28−33] Bolm's works have

Received: April 30, 2024
Revised: July 30, 2024
Accepted: July 31, 2024
Published: August 5, 2024

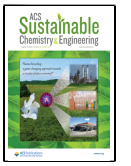

examined the conversion of lignin model compounds representing β-O-4 linkages in base-catalyzed[35] and oxidative reactions.[37] The base-catalyzed reactions produced monomer yields of up to 94%, while the oxidative transformation resulted in aryl-c_α cleavage of the β-O-4 model, resulting in quinone (91% yield) and guaiacol (82% yield) as the two main products. Sievers et al. recently demonstrated hydrogenolysis of the α-O-4 bond in the lignin model compound, benzyl phenyl ether (BPE), over supported Ni catalysts.[43] Due to the similar bond strengths, this ether bond can be considered representative of the β-O-4 linkages found in lignin. In this study, H_2 was continuously flowed through a modified vessel to avoid using a more expensive solid hydrogen source such as $NaBH_4$.[44−46] The study showed full BPE conversion using a commercial Ni (53 wt %) catalyst supported on a silica−alumina support (Ni_{53}/Si−Al) within 3 h and a turnover frequency (TOF) of 0.001 min^{-1}. The present study advances this previously established process by utilizing supported Pd catalysts with improved TOFs up to 0.342 min^{-1}(Figure S3).

The Pd loading of the catalysts was determined by inductively coupled plasma to be 4 wt %, and the catalysts were denoted as Pd_{04}/Al_2O_3 and Pd_{04}/SiO_2. Transmission electron microscopy (TEM) imaging (Figure S4) showed an average Pd particle size of 3.5 nm for Pd_{04}/Al_2O_3 and 7.3 nm for Pd_{04}/SiO_2 before milling, respectively. By comparison, CO chemisorption analysis gave particle sizes of 2.5 nm for Pd_{04}/Al_2O_3 and 4.7 nm for Pd_{04}/SiO_2 (Section S2.5). The calculated dispersion of Pd using CO chemisorption was 45.5% for Pd_{04}/Al_2O_3 and 23.7% for Pd_{04}/SiO_2, while the dispersion values based on TEM were 32.3% and 15.4%. Further characterization of the fresh catalysts can be found in the Supporting Information (SI) including X-ray diffraction (XRD; Section S2.9) and N_2 physisorption (Figure 4).

BPE was milled in combination with one of the catalysts using a Retsch MM400 instrument in a stainless-steel vessel under H_2 flow at atmospheric pressure. Volatile products were collected in a methanol trap during milling while nonvolatile products were quantified by washing the catalyst−feedstock mixture after milling. Gas chromatography with flame ionization detection was used to determine all yields, conversions, and carbon efficiencies. The main two products from hydrogenolysis at the α-carbon and oxygen were toluene and phenol (Scheme 1). The reaction path of mechanocatalytic BPE ether bond cleavage appears to be similar to the one previously shown for the equivalent thermochemical reaction over supported Pd catalysts.[47,48] Hydrogenation of phenol yielded cyclohexanol as a minor product (Section S1.3). We did not observe the hydrogenation of toluene because constant purging allowed toluene to exit the milling vessel before a secondary reaction could occur. Pd_{04}/SiO_2 and Pd_{04}/Al_2O_3 behaved similarly under these conditions. Toluene was produced at a rate of 2.61 and 2.91 mol·min^{-1}, respectively, while phenol yields averaged 48% after 1 h of reaction (Figure 1). By comparison, Ni_{53}/Si−Al produced toluene at a rate of 1.01 mol·min^{-1} over 3 h, with 42% cyclohexanol yield and 17% phenol yield, and the undesired secondary hydrogenation of phenol to cyclohexanol was more prominent.[43] The overall carbon balance of the reaction ranged from 75 to 80% for all three catalysts, and full conversion was observed.

Scheme 1. Reaction Scheme Depicting the Cleavage of BPE Producing Phenol and Toluene Followed by Hydrogenated Products Cyclohexanol and Methylcyclohexane

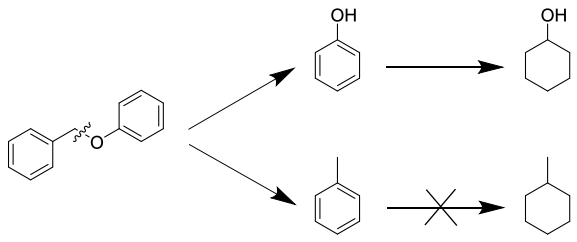

Thermogravimetric analysis (TGA) in air showed a mass loss of 16 wt % for both catalysts, indicating that the unaccounted for carbon was present as an adsorbed species on the catalyst (Section S2.8). Because the deficit in the mass balance aligned well with the mass of carbonaceous deposits on the catalyst, it is suggested that the phenolic moiety from BPE remained chemisorbed on the alumina and silica supports as phenolates, which has been reported for similar catalysts in thermochemical reactions.[49,50] Because Lewis acid sites are the preferred binding sites for these species, pyridine adsorption followed by IR spectroscopy was used to determine the concentration of these sites. For the Pd_{04}/Al_2O_3 catalyst, no Brønsted acid sites were found, while the concentration of Lewis acid sites decreased from 120 μmol·g^{-1} in the fresh catalyst to 1.5 μmol·g^{-1} in the spent one, indicating that the phenolic products saturated the Lewis acid sites on the support (Figures S7 and S8). The phenolic compounds that did not bind after this saturation were easily removed, which resulted in a phenol yield of 48%; minor cyclohexanol yields of 4−6% were also observed due to the hydrogenation of nonadsorbed phenols. While silica supports are generally considered inert, it has been shown that chemisorption of alcohols readily occurs at defect sites that are formed when silica ruptures during milling (Figure S11).[51−53] In addition to chemisorbed phenolates on such defect sites, phenol can physisorb onto silanol sites.[54−56] The physisorbed phenols are more easily removed and comprise most of the phenol yield that was observed after washing. This ultimately suggests that the Lewis acid site concentration plays a minor role in absorption. Lewis acid site occupation accounts for roughly 5% of the unaccounted for phenol for Pd_{04}/Al_2O_3, while defects account for 95%. Pd_{04}/SiO_2 silanol sites and defect sites account for 100% of the missing phenol, considering that the Lewis acid site concentration initially was only 0.012 μmol·g^{-1}. Further calculations are shown in Section S2.7.

Compared to the Ni_{53}/Si−Al catalyst, which had a TOF of 0.001 min^{-1}, the TOFs for Pd_{04}/Al_2O_3 and Pd_{04}/SiO_2 were 0.342 and 0.289 min^{-1}, respectively. We hypothesized that this increase in the TOF is due to the ability of Pd to form interstitial hydrides. These immobilized hydrogen species are expected to be more readily available for reactions during the impact of a ball because they cannot escape to the sides like gaseous H_2 would. Interstitial hydride formation has been extensively used for Pd membranes for H_2 separation.[15−17,57,58] At the surface of Pd membranes or particles, H_2 is able to dissociate into H atoms, which allows hydrogen to easily diffuse into the Pd particle.[16,17,59] These singular H atoms can then be combined with other molecules or compounds on the Pd surface. Many other metals, such a Pt[60] and Ti,[61] can form surface hydrides, but facile hydrogen diffusion into the particle is unique to Pd. Nonconstant changes in the morphology of the Pd particles during milling help to expose reactive hydrides, which are readily available to participate in the hydrogenolysis

https://doi.org/10.1021/acssuschemeng.4c03590
ACS Sustainable Chem. Eng. 2024, 12, 12306−12312

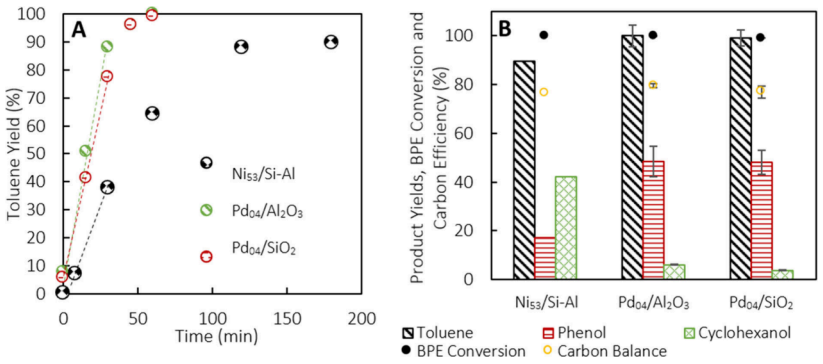

Figure 1. (A) Toluene yields over Ni_{53}/Si−Al, Pd_{04}/SiO_2, and Pd_{04}/Al_2O_3 over 1−3 h of milling and (B) toluene, phenol, cyclohexanol yields, CE, and BPE conversion after the first run. A total of 0.25 g of Pd_{04} catalysts was used at 20 Hz with 0.2 g of BPE and 10 × 10 mm grinding balls at 15 sccm H_2 flow. Alternatively, 1.00 g of Ni_{53}/Si−Al was used with 2 mm × 15 mm balls.

reaction. The presence of this hydrogen reservoir[16] is suggested to significantly increase the efficiency of BPE conversion.

The expected presence of interstitial hydrides was probed by X-ray absorption spectroscopy (XAS; Figure 2).[62] The spectra

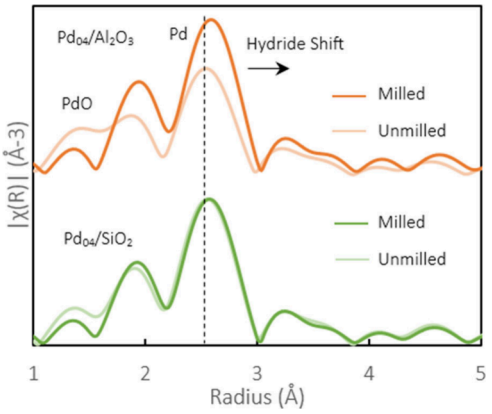

Figure 2. Fourier-transformed *R* space of the experimental Pd K-edge EXAFS signals for Pd_{04}/Al_2O_3 and Pd_{04}/SiO_2 catalysts before and after milling under H_2 to depict hydride formation.

were dominated by metallic Pd (2.5 Å in *R* space), but a contribution of PdO (1.5 Å in *R* space) was clearly visible.[63,64] The spectra of the samples milled in hydrogen showed a decreased contribution of PdO, while the primary peak for Pd−Pd bonds at 2.5 Å increased in intensity for Pd/Al_2O_3 and slightly shifted to a higher bond distance for both catalysts from 2.54 to 2.57 Å. The intensity shifts indicated that hydrogen milling created a sufficiently reducing environment to reduce any oxidized Pd in situ; for Pd_{04}/SiO_2, the Pd present in the fresh sample had a lower PdO concentration, which is why a significant increase in the peak intensity - was not observed, but a slight hydride shift still occurred. This reduction occurred in tandem with the hydrogenolysis reaction, which was promoted by reduced Pd. The rightward shift in the Pd−Pd peak was indicative of hydride formation, which resulted in a slight expansion of the Pd lattice.[16,17,59,63,65,66]

The recyclability of Pd_{04}/Al_2O_3 and Pd_{04}/SiO_2 was tested after calcining the spent catalysts to remove organic residues (Figure 3). Although calcination results in the oxidation of Pd to PdO, it had to be verified that milling under H_2 could restore the reduced Pd particles. EXAFS analysis of spent catalysts after calcination showed a significant increase in the intensity of PdO (1.5 Å) coupled with a reduction in the Pd−Pd bond length (2.5 Å) (Figure S6). After the hydrogenolysis reaction with the recycled catalysts, a shift back to reduced Pd coupled with palladium hydride formation was observed, indicating that milling under H_2 gas flow was able to sufficiently reduce the fresh and recycled Pd catalysts.

With calcination, 88% of Pd_{04}/SiO_2 and 82% of Pd_{04}/Al_2O_3 catalysts were recovered on average. To determine the catalytic

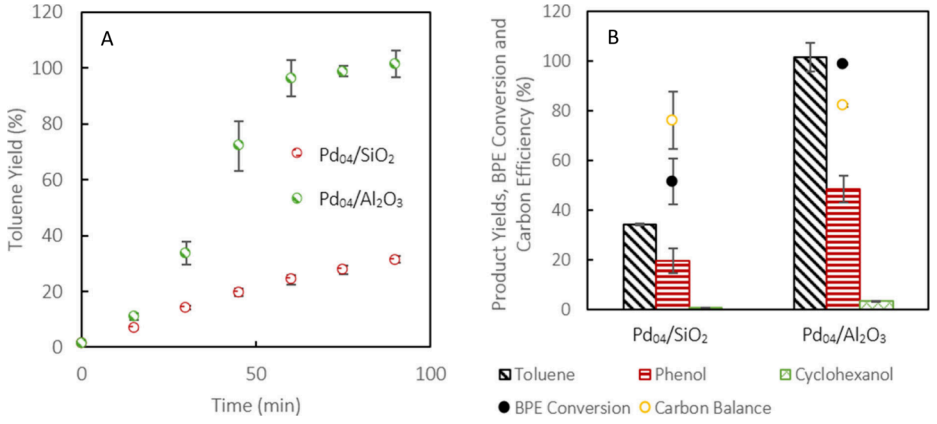

Figure 3. (A) Toluene yields over recycled Pd_{04}/SiO_2 and Pd_{04}/Al_2O_3 over 90 min of milling and (B) total toluene, phenol, cyclohexanol yields, carbon balance, and BPE conversion of recyclability tests for Pd_{04}/Al_2O_3 and Pd_{04}/SiO_2.

https://doi.org/10.1021/acssuschemeng.4c03590
ACS Sustainable Chem. Eng. 2024, 12, 12306−12312

reactivity after calcination, trials were conducted using a combination of recycled and fresh catalysts. To maintain consistency, 0.20 g of the calcined catalyst was combined with 0.05 g of fresh catalyst, resulting in a 4:1 ratio (Figure 3). With Pd_{04}/SiO_2, the maximum toluene yield reached was 34% after 90 min. By comparison, full conversion and a 100% toluene yield was observed with Pd_{04}/Al_2O_3. Phenol production over Pd_{04}/Al_2O_3 was 49%, which was slightly higher than the initial phenol yield over Pd_{04}/Al_2O_3, while the Pd_{04}/SiO_2 yield was much lower, resulting in only 20% (Figure 3B).

Reduced activity of the catalyst can be attributed to a reduced surface area (SA), increased Pd particle size, and alteration of the support throughout the milling process. Initially, Pd_{04}/SiO_2 and Pd_{04}/Al_2O_3 had SAs of 209 and 106 $m^2 \cdot g^{-1}$, respectively (Figure 4). After initial milling, the SA of

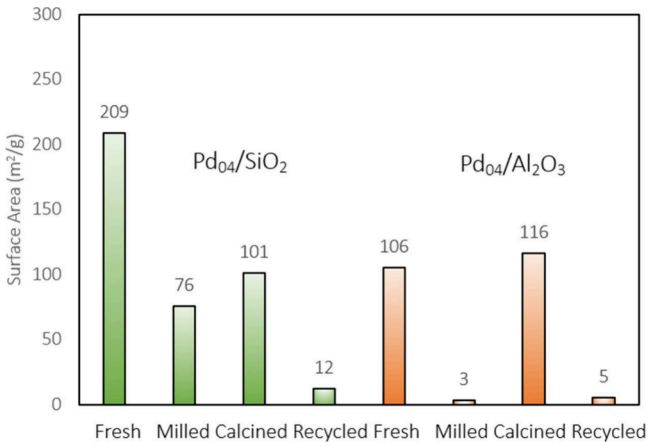

Figure 4. SA analysis of Pd_{04}/SiO_2 and Pd_{04}/Al_2O_3 ($m^2 \cdot g^{-1}$).

Pd_{04}/SiO_2 reduced to 76 $m^2 \cdot g^{-1}$, which increased to 101 $m^2 \cdot g^{-1}$ after calcination. Upon recycling, the catalyst became denser and the SA reduced to 12 $m^2 \cdot g^{-1}$ after milling. The SA of Pd_{04}/Al_2O_3 was drastically reduced to 3 $m^2 \cdot g^{-1}$ after the first reaction but increased to 116 $m^2 \cdot g^{-1}$ after calcination, slightly exceeding the initial value. This partially explains why Pd_{04}/Al_2O_3 was more effective when recycled in comparison to Pd_{04}/SiO_2. TEM images after milling showed the agglomeration of Pd particles (Figure S4). The Pd particles remained active but were less effective compared with the fresh counterparts due to reduced dispersion. For Pd_{04}/Al_2O_3 specifically, amorphization of the Al_2O_3 support was also observed via XRD (Figure S10). Changes in the SiO_2 support structure were more effectively seen with ATR FTIR spectroscopy (Figure S11). The spectra showed the formation of silanol sites and both chemi- and physisorbed interactions between oxygenated products and mechanically activated SiO_2. The combination of these characteristics elucidates how the degradation of these catalysts throughout the milling process affects the recyclability potentials of both Pd_{04}/SiO_2 and Pd_{04}/Al_2O_3.

To illustrate the potential application of mechanocatalytic hydrogenolysis over Pd-based catalysts beyond model compounds, the conversion of supercritical-water-extracted lignin was studied under identical milling conditions. Gel permeation chromatography (GPC) showed significant changes in the average M_w after 1 h of milling (Figure 5). The unmilled lignin showed a significant amount of lignin fragments ranging from 1000 to 30000 $g \cdot mol^{-1}$ (10^3–$10^{4.5}$).

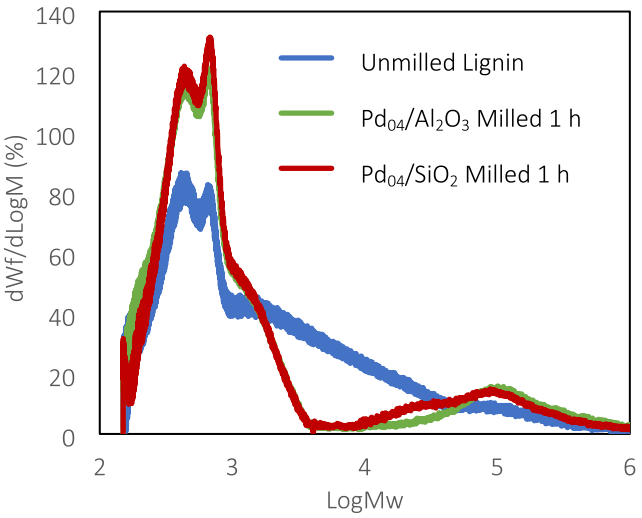

Figure 5. Molecular weight distributions of milled and unmilled lignin determined by GPC.

There were two main peaks, which equate to roughly 430 and 660 $g \cdot mol^{-1}$. The monolignols *p*-coumaryl, coniferyl, and sinapyl alcohol have molar masses of 150, 180, and 210 $g \cdot mol^{-1}$, respectively. Thus, the two peaks are attributed to dimers and trimers, respectively. After milling, the abundance of products with intermediate masses (i.e., 1800–30000 $g \cdot mol^{-1}$) decreased markedly, while the amount of monolignol dimers and trimers increased strongly and small amounts of larger products were formed. As illustrated by the hydrogenolysis of ether bonds in BPE, the reduction in M_w was likely a result of the hydrogenolysis of α-O-4 and β-O-4 bonds. To test this hypothesis, heteronuclear single quantum coherence (HSQC) NMR spectroscopy was conducted to analyze the change in the linkage composition of the supercritical-water-extracted lignin samples that were milled for 1 h using Pd_{04}/Al_2O_3 and Pd_{04}/SiO_2 under the same conditions as BPE. The results (Section S2.11) demonstrate that the abundance of the β-O-4_β linkage was reduced by 5.4% using Pd_{04}/Al_2O_3 and 12.5% for Pd_{04}/SiO_2, using the $\beta\beta_\beta$ peak as a standard. $\beta\beta_\beta$ bond integration was assumed to be unaffected by the catalysts in a hydrogenolysis environment, where the integral of the peak remained constant before and after milling. This ultimately shows that this approach is feasible with real lignin, and with additional optimization and longer milling conditions, lignin could be converted with a high depolymerization efficacy.

In summary, this work demonstrates the potential of using Pd-based catalysts for the hydrogenolysis of lignin in a mechanocatalytic environment. Using Pd as the primary metal in these heterogeneous catalysts provided superior activity compared to that of Ni-based catalysts used under the same conditions. The ability of Pd to form interstitial hydrides that readily participate in hydrogenolysis reactions enhances the rate of successful collisions. Chemisorption of phenolates has been identified as a remaining challenge of this process.

■ ASSOCIATED CONTENT

Supporting Information

The Supporting Information is available free of charge at https://pubs.acs.org/doi/10.1021/acssuschemeng.4c03590.

https://doi.org/10.1021/acssuschemeng.4c03590
ACS Sustainable Chem. Eng. 2024, 12, 12306−12312

Full experimental details and analytical data including TOF and particle percent dispersion calculations, TEM images, XANES/EXAFS spectra, XRD, pyridine adsorption concentrations along with FTIR spectra, TGA, FTIR analysis conducted using an ATR attachment, and 2D HSQC NMR of the lignin samples before and after milling (PDF)

AUTHOR INFORMATION

Corresponding Author

Carsten Sievers − *School of Chemistry and Biochemistry and School of Chemical and Biomolecular Engineering, Georgia Institute of Technology, Atlanta, Georgia 30332, United States;* orcid.org/0000-0002-5713-1875; Email: carsten.sievers@chbe.gatech.edu

Authors

Erin V. Phillips − *School of Chemistry and Biochemistry, Georgia Institute of Technology, Atlanta, Georgia 30332, United States*

Andrew W. Tricker − *Independent Researcher, Washington, D.C. 20009, United States;* orcid.org/0000-0001-5526-1249

Eli Stavitski − *National Synchrotron Light Source II, Brookhaven National Laboratory, Upton, New York 11973, United States;* orcid.org/0000-0002-3337-2930

Marta Hatzell − *School of Chemical and Biomolecular Engineering, Georgia Institute of Technology, Atlanta, Georgia 30332, United States; George W. Woodruff School of Mechanical Engineering, Atlanta, Georgia 30318, United States;* orcid.org/0000-0002-5144-4969

Complete contact information is available at: https://pubs.acs.org/10.1021/acssuschemeng.4c03590

Notes

The authors declare no competing financial interest.

ACKNOWLEDGMENTS

This research was supported by the Renewable Bioproducts Institute through the Paper and Science Engineering Fellowship and the U.S. National Science Foundation under Grant 2028998. This research used Inner Shell Spectroscopy beamline (ISS, 8-ID) of the National Synchrotron Light Source II, a U.S. Department of Energy (DOE), Office of Science User Facility, operated for the DOE, Office of Science, by Brookhaven National Laboratory under Contract DE-SC0012704.

REFERENCES

(1) Chio, C.; Sain, M.; Qin, W. Lignin utilization: a review of lignin depolymerization from various aspects. *Renewable and Sustainable Energy Reviews* **2019**, *107*, 232−249.

(2) Cheng, C.; Wang, J.; Shen, D.; Xue, J.; Guan, S.; Gu, S.; Luo, K. H. Catalytic Oxidation of Lignin in Solvent Systems for Production of Renewable Chemicals: A Review. *Polymers (Basel)* **2017**, *9*, 240.

(3) Lahive, C. W.; Kamer, P. C. J.; Lancefield, C. S.; Deuss, P. J. An Introduction to Model Compounds of Lignin Linking Motifs; Synthesis and Selection Considerations for Reactivity Studies. *ChemSusChem* **2020**, *13*, 4238−4265.

(4) Schutyser, W.; Renders, T.; Van den Bosch, S.; Koelewijn, S. F.; Beckham, G. T.; Sels, B. F. Chemicals from lignin: an interplay of lignocellulose fractionation, depolymerisation, and upgrading. *Chem. Soc. Rev.* **2018**, *47*, 852−908.

(5) Rinaldi, R.; Jastrzebski, R.; Clough, M. T.; Ralph, J.; Kennema, M.; Bruijnincx, P. C.; Weckhuysen, B. M. Paving the Way for Lignin Valorisation: Recent Advances in Bioengineering, Biorefining and Catalysis. *Angew. Chem., Int. Ed. Engl.* **2016**, *55*, 8164−215.

(6) Mu, W.; Ben, H.; Ragauskas, A.; Deng, Y. Lignin Pyrolysis Components and Upgrading—Technology Review. *BioEnergy Research* **2013**, *6*, 1183−1204.

(7) Li, C.; Zhao, X.; Wang, A.; Huber, G. W.; Zhang, T. Catalytic Transformation of Lignin for the Production of Chemicals and Fuels. *Chem. Rev.* **2015**, *115*, 11559−624.

(8) Awan, I. Z.; Tanchoux, N.; Quignard, F.; Albonetti, S.; Cavani, F.; Di Renzo, F. Heterogeneous Catalysis as a Tool for Production of Aromatic Compounds From Lignin. *Horizons in Sustainable Industrial Chemistry and Catalysis* **2019**, *178*, 257−275.

(9) Zhang, H.; Fu, S.; Du, X.; Deng, Y. Advances in Versatile Nanoscale Catalyst for the Reductive Catalytic Fractionation of Lignin. *ChemSusChem* **2021**, *14*, 2268−2294.

(10) Wang, H.; Pu, Y.; Ragauskas, A.; Yang, B. From lignin to valuable products-strategies, challenges, and prospects. *Bioresour. Technol.* **2019**, *271*, 449−461.

(11) Qiu, S.; Wang, M.; Fang, Y.; Tan, T. Reductive catalytic fractionation of lignocellulose: when should the catalyst meet depolymerized lignin fragments? *Sustainable Energy & Fuels* **2020**, *4*, 5588−5594.

(12) Liu, X.; Bouxin, F. P.; Fan, J.; Budarin, V. L.; Hu, C.; Clark, J. H. Recent Advances in the Catalytic Depolymerization of Lignin towards Phenolic Chemicals: A Review. *ChemSusChem* **2020**, *13*, 4296−4317.

(13) Yang, L.; Seshan, K.; Li, Y. A review on thermal chemical reactions of lignin model compounds. *Catal. Today* **2017**, *298*, 276−297.

(14) Yang, H.; Strien, J. R. J.; Chowdari, R. K.; Wang, Z.; Heeres, H. J.; Deuss, P. J. Enhanced Catalytic Depolymerization of a Kraft Lignin by a Mechanochemical Approach. *Energy Fuels* **2022**, *36*, 6606−6610.

(15) Oh, D. K.; Lee, K. Y.; Park, J. S. Hydrogen Purification from Compact Palladium Membrane Module Using a Low Temperature Diffusion Bonding Technology. *Membranes* **2020**, *10*, 338.

(16) Fovanna, T.; Nachtegaal, M.; Clark, A. H.; Kröcher, O.; Ferri, D. Preparation, Quantification, and Reaction of Pd Hydrides on Pd/Al2O3 in Liquid Environment. *ACS Catal.* **2023**, *13*, 3323−3332.

(17) Tew, M. W.; Nachtegaal, M.; Janousch, M.; Huthwelker, T.; van Bokhoven, J. A. The irreversible formation of palladium carbide during hydrogenation of 1-pentyne over silica-supported palladium nanoparticles: in situ Pd K and L3 edge XAS. *Phys. Chem. Chem. Phys.* **2012**, *14*, 5761−8.

(18) Howard, J. L.; Cao, Q.; Browne, D. L. Mechanochemistry as an emerging tool for molecular synthesis: what can it offer? *Chem. Sci.* **2018**, *9*, 3080−3094.

(19) Tricker, A. W.; Samaras, G.; Hebisch, K. L.; Realff, M. J.; Sievers, C. Hot spot generation, reactivity, and decay in mechanochemical reactors. *Chem. Eng. J.* **2020**, *382*, 122954.

(20) Amirjalayer, S.; Fuchs, H.; Marx, D. Understanding the Mechanocatalytic Conversion of Biomass: A Low-Energy One-Step Reaction Mechanism by Applying Mechanical Force. *Angew. Chem., Int. Ed. Engl.* **2019**, *58*, 5232−5235.

(21) Takacs, L. The historical development of mechanochemistry. *Chem. Soc. Rev.* **2013**, *42*, 7649−59.

(22) Giannakoudakis, D. A.; Chatel, G.; Colmenares, J. C. Mechanochemical Forces as a Synthetic Tool for Zero- and One-Dimensional Titanium Oxide-Based Nano-photocatalysts. *Top Curr. Chem. (Z)* **2020**, *378*, 2.

(23) Reichle, S.; Felderhoff, M.; Schuth, F. Mechanocatalytic Room-Temperature Synthesis of Ammonia from Its Elements Down to Atmospheric Pressure. *Angew. Chem., Int. Ed. Engl.* **2021**, *60*, 26385−26389.

(24) Kulla, H.; Wilke, M.; Fischer, F.; Rollig, M.; Maierhofer, C.; Emmerling, F. Warming up for mechanosynthesis - temperature development in ball mills during synthesis. *Chem. Commun. (Camb)* **2017**, *53*, 1664−1667.

(25) Liu, X.; Li, Y.; Zeng, L.; Li, X.; Chen, N.; Bai, S.; He, H.; Wang, Q.; Zhang, C. A Review on Mechanochemistry: Approaching Advanced Energy Materials with Greener Force. *Adv. Mater.* **2022**, *34*, No. e2108327.
(26) Fischer, F.; Wenzel, K. J.; Rademann, K.; Emmerling, F. Quantitative determination of activation energies in mechanochemical reactions. *Phys. Chem. Chem. Phys.* **2016**, *18*, 23320−5.
(27) Immohr, S.; Felderhoff, M.; Weidenthaler, C.; Schuth, F. An orders-of-magnitude increase in the rate of the solid-catalyzed CO oxidation by in situ ball milling. *Angew. Chem., Int. Ed. Engl.* **2013**, *52*, 12688−91.
(28) Hilgert, J.; Meine, N.; Rinaldi, R.; Schüth, F. Mechanocatalytic depolymerization of cellulose combined with hydrogenolysis as a highly efficient pathway to sugar alcohols. *Energy Environ. Sci.* **2013**, *6*, 92−96.
(29) Schüth, F.; Rinaldi, R.; Meine, N.; Käldström, M.; Hilgert, J.; Rechulski, M. D. K. Mechanocatalytic depolymerization of cellulose and raw biomass and downstream processing of the products. *Catal. Today* **2014**, *234*, 24−30.
(30) Kaufman Rechulski, M. D.; Käldström, M.; Richter, U.; Schüth, F.; Rinaldi, R. Mechanocatalytic Depolymerization of Lignocellulose Performed on Hectogram and Kilogram Scales. *Ind. Eng. Chem. Res.* **2015**, *54*, 4581−4592.
(31) Käldström, M.; Meine, N.; Farès, C.; Schüth, F.; Rinaldi, R. Deciphering 'water-soluble lignocellulose' obtained by mechanocatalysis: new insights into the chemical processes leading to deep depolymerization. *Green Chem.* **2014**, *16*, 3528−3538.
(32) Calvaruso, G.; Clough, M. T.; Rinaldi, R. Biphasic extraction of mechanocatalytically-depolymerized lignin from water-soluble wood and its catalytic downstream processing. *Green Chem.* **2017**, *19*, 2803−2811.
(33) Carrasquillo-Flores, R.; Käldström, M.; Schüth, F.; Dumesic, J. A.; Rinaldi, R. Mechanocatalytic Depolymerization of Dry (Ligno)-cellulose As an Entry Process for High-Yield Production of Furfurals. *ACS Catal.* **2013**, *3*, 993−997.
(34) Kessler, M.; Rinaldi, R. Kinetic Energy Dose as a Unified Metric for Comparing Ball Mills in the Mechanocatalytic Depolymerization of Lignocellulose. *Front. Chem.* **2022**, *9*, No. 816553.
(35) Kleine, T.; Buendia, J.; Bolm, C. Mechanochemical degradation of lignin and wood by solvent-free grinding in a reactive medium. *Green Chem.* **2013**, *15*, 160−166.
(36) Weissbach, U.; Dabral, S.; Konnert, L.; Bolm, C.; Hernandez, J. G. Selective enzymatic esterification of lignin model compounds in the ball mill. *Beilstein J. Org. Chem.* **2017**, *13*, 1788−1795.
(37) Dabral, S.; Wotruba, H.; Hernández, J. G.; Bolm, C. Mechanochemical Oxidation and Cleavage of Lignin β-O-4 Model Compounds and Lignin. *ACS Sustainable Chem. Eng.* **2018**, *6*, 3242−3254.
(38) Zhang, Q.; Jerome, F. Mechanocatalytic deconstruction of cellulose: an emerging entry into biorefinery. *ChemSusChem* **2013**, *6*, 2042−4.
(39) Barakat, A.; Jerome, F.; Rouau, X. A dry platform for separation of proteins from biomass-containing polysaccharides, lignin, and polyphenols. *ChemSusChem* **2015**, *8*, 1161−6.
(40) Karam, A.; Amaniampong, P. N.; Garcia Fernandez, J. M.; Oldani, C.; Marinkovic, S.; Estrine, B.; De Oliveira Vigier, K.; Jerome, F. Mechanocatalytic Depolymerization of Cellulose With Perfluorinated Sulfonic Acid Ionomers. *Front. Chem.* **2018**, *6*, 74.
(41) Sierra Cantor, J. F.; De Oliveira Vigier, K.; Labat, G.; Da Silva Perez, D.; Jérôme, F. Mechanocatalytic depolymerization of hemicellulose to low molecular weight oligosaccharides over an aquivion ionomer. *RSC Sustainability* **2023**, *1*, 446−453.
(42) Tricker, A. W.; Stellato, M. J.; Kwok, T. T.; Kruyer, N. S.; Wang, Z.; Nair, S.; Thomas, V. M.; Realff, M. J.; Bommarius, A. S.; Sievers, C. Similarities in Recalcitrant Structures of Industrial Non-Kraft and Kraft Lignin. *ChemSusChem* **2020**, *13*, 4624−4632.
(43) Tricker, A. W.; Najmi, S.; Phillips, E. V.; Hebisch, K. L.; Kang, J. X.; Sievers, C. Mechanocatalytic hydrogenolysis of benzyl phenyl ether over supported nickel catalysts. *RCS Sustainability* **2023**, *1*, 346.
(44) Nagy, M.; David, K.; Britovsek, G. J. P.; Ragauskas, A. J. Catalytic hydrogenolysis of ethanol organosolv lignin. *hfsg* **2009**, *63*, 513−520.
(45) Jiang, B.; Hu, J.; Qiao, Y.; Jiang, X.; Lu, P. Depolymerization of Lignin over a Ni−Pd Bimetallic Catalyst Using Isopropanol as an in Situ Hydrogen Source. *Energy Fuels* **2019**, *33*, 8786−8793.
(46) Galkin, M. V.; Dahlstrand, C.; Samec, J. S. Mild and Robust Redox-Neutral Pd/C-Catalyzed Lignol beta-O-4′ Bond Cleavage Through a Low-Energy-Barrier Pathway. *ChemSusChem* **2015**, *8*, 2187−92.
(47) Mauriello, F.; Ariga-Miwa, H.; Paone, E.; Pietropaolo, R.; Takakusagi, S.; Asakura, K. Transfer hydrogenolysis of aromatic ethers promoted by the bimetallic Pd/Co catalyst. *Catal. Today* **2020**, *357*, 511−517.
(48) Kim, J. K.; Lee, J. K.; Kang, K. H.; Song, J. C.; Song, I. K. Selective cleavage of C O bond in benzyl phenyl ether to aromatics over Pd−Fe bimetallic catalyst supported on ordered mesoporous carbon. *Applied Catalysis A: General* **2015**, *498*, 142−149.
(49) Foo, G. S.; Rogers, A. K.; Yung, M. M.; Sievers, C. Steric Effect and Evolution of Surface Species in the Hydrodeoxygenation of Bio-Oil Model Compounds over Pt/HBEA. *ACS Catal.* **2016**, *6*, 1292−1307.
(50) Stellato, M. J.; Innocenti, G.; Bommarius, A. S.; Sievers, C. Pore Blocking by Phenolates as Deactivation Path during the Cracking of 4-Propylphenol over ZSM-5. *Catalysts* **2021**, *11*, 721.
(51) Pan, W.; Zhong, W.; Zhang, D.; Liu, C. Theoretical study of the reactions of 2-chlorophenol over the dehydrated and hydroxylated silica clusters. *J. Phys. Chem. A* **2012**, *116*, 430−6.
(52) Popov, A.; Kondratieva, E.; Gilson, J.-P.; Mariey, L.; Travert, A.; Maugé, F. IR study of the interaction of phenol with oxides and sulfided CoMo catalysts for bio-fuel hydrodeoxygenation. *Catal. Today* **2011**, *172*, 132−135.
(53) Nakashima, Y.; Fukushima, M.; Hyuga, H. Surface modification of silica powder by mild ball milling. *Colloids Surf., A* **2022**, *652*, 129828.
(54) Berro, Y.; Gueddida, S.; Lebègue, S.; Pasc, A.; Canilho, N.; Kassir, M.; Hassan, F. E. H.; Badawi, M. Atomistic description of phenol, CO and H2O adsorption over crystalline and amorphous silica surfaces for hydrodeoxygenation applications. *Appl. Surf. Sci.* **2019**, *494*, 721−730.
(55) Gueddida, S.; Lebègue, S.; Badawi, M. Assessing the Potential of Amorphous Silica Surfaces for the Removal of Phenol from Biofuel: A Density Functional Theory Investigation. *J. Phys. Chem. C* **2020**, *124*, 20262−20269.
(56) Nöske, M.; Breitung-Faes, S.; Kwade, A. Electrostatic Stabilization and Characterization of Fine Ground Silicon Particles in Ethanol. *Silicon* **2019**, *11*, 3001−3010.
(57) Nicholson, K. M.; Chandrasekhar, N.; Sholl, D. S. Powered by DFT: Screening methods that accelerate materials development for hydrogen in metals applications. *Acc. Chem. Res.* **2014**, *47*, 3275−83.
(58) Kamakoti, P.; Morreale, B. D.; Ciocco, M. V.; Howard, B. H.; Killmeyer, R. P.; Cugini, A. V.; Sholl, D. S. Prediction of Hydrogen FluxThrough Sulfur-Tolerant BinaryAlloy Membranes. *Science* **2005**, *307*, 569−573.
(59) Stakheev, A. Y.; Mashkovskii, I. C.; Tkachenko, O. P.; Klementiev, K. V.; Grünert, W.; Baeva, G. N.; Kustov, L. M. Formation of palladium hydride nanoparticles in Pd/C catalyst as evidenced by in situ XAS data. *Russian Chemical Bulletin* **2009**, *58*, 280−283.
(60) Scheler, T.; Degtyareva, O.; Marqués, M.; Guillaume, C. L.; Proctor, J. E.; Evans, S.; Gregoryanz, E. Synthesis and properties of platinum hydride. *Phys. Rev. B* **2011**, *83*. DOI: 10.1103/PhysRevB.83.214106
(61) Kobayashi, Y.; Tang, Y.; Kageyama, T.; Yamashita, H.; Masuda, N.; Hosokawa, S.; Kageyama, H. Titanium-Based Hydrides as Heterogeneous Catalysts for Ammonia Synthesis. *J. Am. Chem. Soc.* **2017**, *139*, 18240−18246.
(62) Leshchev, D.; Rakitin, M.; Luvizotto, B.; Kadyrov, R.; Ravel, B.; Attenkofer, K.; Stavitski, E. The Inner Shell Spectroscopy beamline at

NSLS-II: a facility for in situ and operando X-ray absorption spectroscopy for materials research. *J. Synchrotron Radiat* **2022**, *29*, 1095−1106.
(63) Fovanna, T.; Alxneit, I.; Clark, A. H.; Checchia, S.; Di Michiel, M.; Kröcher, O.; Nachtegaal, M.; Ferri, D. Reduction of PdO/Al2O3 in Liquid Cyclohexane Followed In Situ by ATR-IR, High-Energy XRD, and XAS. *J. Phys. Chem. C* **2021**, *125*, 16473−16482.
(64) Lopes, C. W.; Cerrillo, J. L.; Palomares, A. E.; Rey, F.; Agostini, G. An in situ XAS study of the activation of precursor-dependent Pd nanoparticles. *Phys. Chem. Chem. Phys.* **2018**, *20*, 12700−12709.
(65) Guan, E.; Foucher, A. C.; Marcella, N.; Shirman, T.; Luneau, M.; Head, A. R.; Verbart, D. M. A.; Aizenberg, J.; Friend, C. M.; Stacchiola, D.; Stach, E. A.; Frenkel, A. I. New Role of Pd Hydride as a Sensor of Surface Pd Distributions in Pd−Au Catalysts. *ChemCatChem.* **2020**, *12*, 717−721.
(66) Bugaev, A. L.; Guda, A. A.; Lazzarini, A.; Lomachenko, K. A.; Groppo, E.; Pellegrini, R.; Piovano, A.; Emerich, H.; Soldatov, A. V.; Bugaev, L. A.; Dmitriev, V. P.; van Bokhoven, J. A.; Lamberti, C. In situ formation of hydrides and carbides in palladium catalyst: When XANES is better than EXAFS and XRD. *Catal. Today* **2017**, *283*, 119−126.

https://doi.org/10.1021/acssuschemeng.4c03590
ACS Sustainable Chem. Eng. 2024, 12, 12306−12312